

# Determination of the Newtonian Gravitational Constant Using Atom Interferometry

G. Lamporesi<sup>1</sup>, A. Bertoldi<sup>1</sup>, L. Cacciapuoti<sup>2</sup>, M. Prevedelli<sup>3</sup>, and G.M. Tino<sup>1\*</sup>

<sup>1</sup>*Dipartimento di Fisica and LENS, Università di Firenze - INFN  
Sezione di Firenze, Via Sansone 1, 50019 Sesto Fiorentino, Italy*

<sup>2</sup>*ESA Research and Scientific Support Department, ESTEC,  
Keplerlaan 1 - P.O. Box 299, 2200 AG Noordwijk ZH, The Netherlands*

<sup>3</sup>*Dipartimento di Chimica Fisica e Inorganica, Università di Bologna, V.le del Risorgimento 4, 40136 Bologna, Italy*

(Dated: February 9, 2022)

We present a new measurement of the Newtonian gravitational constant  $G$  based on cold atom interferometry. Freely falling samples of laser-cooled rubidium atoms are used in a gravity gradiometer to probe the field generated by nearby source masses. In addition to its potential sensitivity, this method is intriguing as gravity is explored by a quantum system. We report a value of  $G = 6.667 \cdot 10^{-11} \text{ m}^3 \text{ kg}^{-1} \text{ s}^{-2}$ , estimating a statistical uncertainty of  $\pm 0.011 \cdot 10^{-11} \text{ m}^3 \text{ kg}^{-1} \text{ s}^{-2}$  and a systematic uncertainty of  $\pm 0.003 \cdot 10^{-11} \text{ m}^3 \text{ kg}^{-1} \text{ s}^{-2}$ . The long-term stability of the instrument and the signal-to-noise ratio demonstrated here open interesting perspectives for pushing the measurement accuracy below the 100 ppm level.

The Newtonian constant of gravity  $G$  is one of the most measured fundamental physical constants and at the same time the least precisely known. Improving the knowledge of  $G$  has not only a pure metrological interest, but is also important for the key role that it plays in theories of gravitation, cosmology, particle physics, in geophysical models, and astrophysical observations. However, the extreme weakness of the gravitational force and the impossibility of shielding the effects of gravity make it difficult to measure  $G$ , while keeping systematic effects well under control. Many of the measurements performed to date are based on the traditional torsion pendulum method [1], direct derivation of the historical experiment performed by Cavendish in 1798. Recently, many groups have set up new experiments based on different concepts and with completely different systematics: a beam-balance system [2], a laser interferometry measurement of the acceleration of a freely falling test mass [3], experiments based on Fabry-Perot or microwave cavities [4, 5]. However, the most precise measurements available today still show substantial discrepancies, limiting the accuracy of the 2006 CODATA recommended value for  $G$  to 1 part in  $10^4$ . From this point of view, the realization of conceptually different experiments can help to identify still hidden systematic effects and therefore improve the confidence in the final result.

Cold-atom interferometry has demonstrated outstanding performances for the measurement of tiny rotations and accelerations and it is widely used for many applications: precision measurements of gravity [6], gravity gradient [7], and rotation of the Earth [8, 9], but also tests of the Einstein's weak equivalence principle [10], tests of the Newton's law at short distances [11], and measurement of fundamental physical constants [12, 13]. Applications of these techniques for fundamental physics experiments in space are under study [14].

In this paper, we present a new determination of the Newtonian constant of gravity based on cold-atom in-

terferometry. An atomic gravity gradiometer is used to measure the differential acceleration experienced by two freely falling samples of laser-cooled rubidium atoms under the influence of nearby tungsten masses. The measurement is repeated in two different configurations of the source masses and modeled by a numerical simulation. From the evolution of the atomic wavepackets and the distribution of the source masses, we evaluate the expected differential acceleration, having  $G$  as unique free parameter. A value for the Newton's constant of gravity is finally extracted by comparing experimental data and numerical simulations. Proof-of-principle experiments with similar schemes using lead masses were already presented in [15, 16]. In the present work, specific efforts have been devoted to the control of systematic effects related to atomic trajectories, positioning of source masses, and stray fields. In particular, the high density of tungsten is crucial in our experiment to compensate for the Earth gravity gradient. In both configurations of the source masses, atom interferometers can therefore be operated in spatial regions where the overall acceleration is slowly varying and the sensitivity of the measurement to the initial position and velocity of the atoms strongly reduced.

Our atom interferometer uses light pulses to stimulate  $^{87}\text{Rb}$  atoms on the two-photon Raman transition between the hyperfine levels  $F = 1$  and  $F = 2$  of the ground state [17]. The light field is generated by two counter-propagating laser beams with wave vectors  $\mathbf{k}_1$  and  $\mathbf{k}_2 \simeq -\mathbf{k}_1$  aligned along the vertical axis. Atoms interact with the Raman lasers on the three-pulse sequence  $\pi/2 - \pi - \pi/2$  which splits, redirects, and recombines the atomic wavepackets. At the end of the interferometer, the probability of detecting the atoms in the state  $F = 2$  is given by  $P_2 = 1/2 \cdot (1 - \cos \Phi)$ , where  $\Phi$  represents the phase difference accumulated by the wavepackets along the two interferometer arms. In the presence of a gravity field, atoms experience a phase

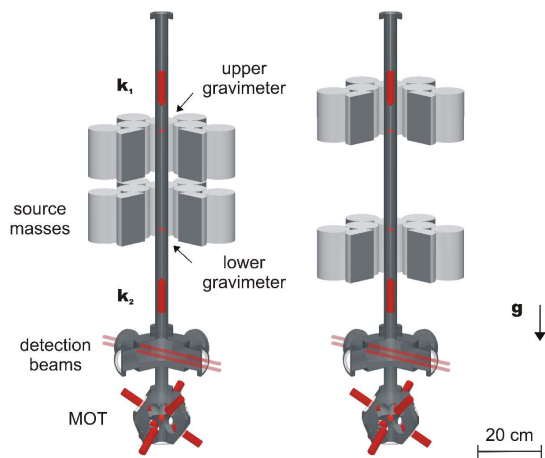


FIG. 1: Schematic of the experiment showing the gravity gradiometer set-up with the Raman beams propagating along the vertical direction. During the  $G$  measurement, the position of the source masses is alternated between configuration  $C_1$  (left) and  $C_2$  (right).

shift  $\Phi = (\mathbf{k}_1 - \mathbf{k}_2) \cdot \mathbf{g} T^2$  depending on the local gravitational acceleration  $\mathbf{g}$  [18]. The gravity gradiometer consists of two absolute accelerometers operated in differential mode. Two spatially separated atomic clouds in free fall along the same vertical axis are simultaneously interrogated by the same Raman beams to provide a measurement of the differential acceleration induced by gravity on the two samples.

Figure 1 shows a schematic of the experiment. The gravity gradiometer set-up and the configurations of the source masses ( $C_1$  and  $C_2$ ) used for the  $G$  measurement are visible. Further details on the atom interferometer apparatus and the source masses assembly can be found in [15, 19]. A magneto-optical trap (MOT) with beams oriented in a 1-1-1 configuration collects rubidium atoms from the background vapor of the chamber at the bottom of the apparatus. Using the moving molasses technique, the sample is launched vertically along the symmetry axis of the vacuum tube and cooled down to a temperature of  $2.5 \mu\text{K}$ . The gravity gradient is probed by two atomic clouds moving in free flight along the vertical axis of the apparatus and simultaneously reaching the apogees of their ballistic trajectories at 60 cm and 90 cm above the MOT. Such a geometry, requiring the preparation and the launch of two samples with high atom numbers in a time interval of about 100 ms, is achieved by juggling the atoms loaded in the MOT: A first cloud of  $10^9$  atoms is launched to 80 cm above the MOT; during its ballistic flight,  $5 \cdot 10^8$  atoms are loaded and launched to 90 cm; finally, the first cloud is recaptured in the MOT and launched again to a height of 60 cm. Shortly after this sequence, the two atomic samples are velocity selected and prepared in the ( $F = 1, m_F = 0$ ) level. The interferom-

eters take place at the center of the vertical tube shown in Fig. 1. In this region, surrounded by a system of two  $\mu$ -metal shields (76 dB attenuation factor in the axial direction), a uniform magnetic field of  $\sim 250$  mG along the vertical direction defines the quantization axis. The field gradient along this axis is lower than  $5 \cdot 10^{-5}$  G/mm. The population of the ground state is measured in the chamber placed just above the MOT by selectively exciting the atoms on the  $F = 1, 2$  hyperfine levels and detecting the light-induced fluorescence emission. We typically detect  $10^5$  atoms on each rubidium sample after the interferometer sequence.

The Raman beams are generated by two extended-cavity diode lasers and amplified in a tapered amplifier. An optical phase-locked loop keeps their frequency difference in resonance with the transition between the two hyperfine levels of the  $^{87}\text{Rb}$  ground state ( $\sim 6.8$  GHz) and stabilizes their relative phase to about 100 mrad (rms) in a 5 Hz–10 MHz bandwidth [20]. The two co-propagating beams enter the vacuum system from the bottom of the MOT cell with the same linear polarization, travel along the axis of the vertical tube and, after crossing a quarter-wave plate, are reflected back producing a *lin* $\perp$ *lin* polarization scheme. Their frequency difference is ramped down with continuous phase during the experiment cycle to compensate for the Doppler effect and ensure that freely falling atoms remain resonant with the laser light. In this way, only one pair of counterpropagating laser beams with crossed linear polarizations is able to stimulate the atoms on the two-photon transition. The three-pulse interferometer has a duration of  $2T = 320$  ms. The  $\pi$  pulse lasts  $48 \mu\text{s}$  and occurs 5 ms after the atomic clouds reach their apogees. Therefore, during the  $\pi/2 - \pi - \pi/2$  pulse sequence, atomic trajectories are almost symmetric with respect to the apogees, allowing a better control of systematic effects induced by spurious magnetic fields.

The source masses [19] are composed of 24 tungsten alloy (INERMET IT180) cylinders, for a total mass of about 516 kg. They are positioned on two titanium platforms and distributed in hexagonal symmetry around the vertical axis of the tube (see Fig. 1). Each cylinder is machined to a diameter of 100.00 mm and a height of 150.20 mm after a hot isostatic pressing treatment applied to compress the material and reduce density inhomogeneities. The internal structure of the material has been analyzed using different methods: ultrasonic tests, microscope analysis, and surface studies. Finally, a destructive test has been performed to characterize the density distribution. We have measured a maximum density variation of  $2.6 \cdot 10^{-3}$  and an average density inhomogeneity of  $6.6 \cdot 10^{-4}$  over volume samples of about 1/40 of the whole cylinder volume.

To evaluate the stability of the gravity gradiometer, we performed a 5-hour measurement run in which the differential phase shift was continuously monitored. Each atom interferometer in the gravity gradiometer measures

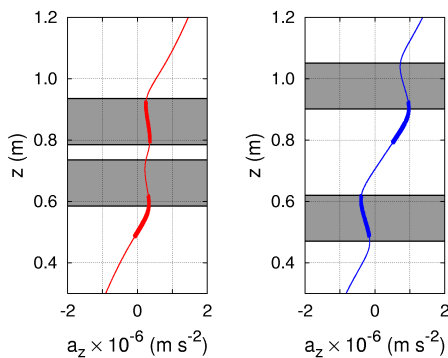


FIG. 2: Acceleration along the symmetry axis of the system in configuration  $C_1$  (left) and  $C_2$  (right). The simulation includes the effect of the source masses and the Earth gravity gradient. The spatial extension of the atomic trajectories for the upper and lower interferometers is indicated by the thick lines. The shaded regions show the positions of the source masses.

the local acceleration with respect to the common reference frame identified by the wavefronts of the Raman lasers. Therefore, even if the phase noise induced by vibrations on the retro-reflecting mirror completely washes out the atom interference fringes, the signals simultaneously detected on the upper and lower accelerometer remain coupled and preserve a fixed phase relation. As a consequence, when the trace of the upper accelerometer is plotted as a function of the lower one, experimental points distribute along an ellipse. The differential phase shift is then obtained from the eccentricity and the rotation angle of the ellipse fitting the data [21]. We have evaluated the Allan variance of the differential phase shift and verified that it decays as the inverse of the integration time, showing the typical behavior expected for white noise. The instrument has a sensitivity of 140 mrad at 1 s of integration time, corresponding to a sensitivity to differential accelerations of  $3.5 \cdot 10^{-8} g$  in 1 s. These performances are compatible with a numerical simulation assuming quantum-projection-noise-limited detection with  $10^5$  atoms.

The Newtonian gravitational constant has been obtained from a series of gravity gradient measurements performed by periodically changing the vertical position of the source masses between configuration  $C_1$  and  $C_2$ , with the atoms always launched along the same trajectories. Figure 2 shows the acceleration along the symmetry axis for both configurations. Because of the high density of tungsten, the gravitational field produced by the source masses is able to compensate for the Earth gravity gradient. Operating the interferometers close to these stationary points reduces the uncertainty on  $G$  due to the knowledge of the atomic positions by two orders of magnitude. A typical data sequence used for the measurement of  $G$  is shown in Fig. 3. Each phase measure-

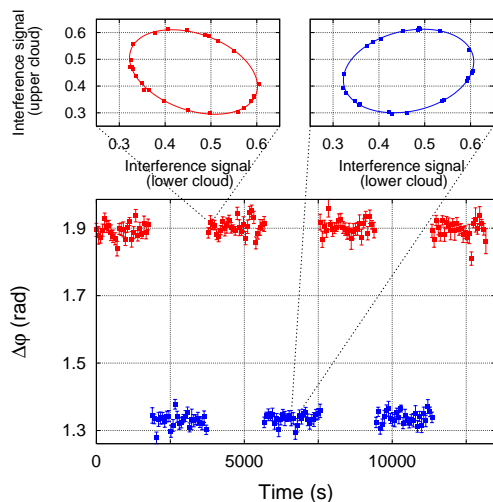


FIG. 3: Typical data set showing the modulation of the differential phase shift measured by the atomic gravity gradiometer when the distribution of the source masses is alternated between configuration  $C_1$  (red squares) and  $C_2$  (blue squares). Each phase measurement is obtained by fitting a 24-point scan of the atom interference fringes to an ellipse.

ment is obtained by fitting a 24-point scan of the atom interference fringes to an ellipse. The modulation on the differential phase shift measured by the gravity gradiometer can be resolved with a signal-to-noise ratio of 180 after about one hour. Experimental data have been collected during two separate measurement runs performed in February and May 2007.

The differential nature of the measurement ensures an efficient rejection of many systematic errors: Firstly, each gravity gradient measurement is highly insensitive to phase shifts appearing in common mode on the two interferometers [7]; in addition, the differential measurement performed by alternating the source masses between configuration  $C_1$  and  $C_2$  removes effects not depending on the masses position. A budget of the systematic errors affecting the value of  $G$  is presented in Table I. Each effect is taken into account in our numerical simulation and its contribution evaluated on the basis of the measurements performed on the relevant parameters. Positioning errors account for uncertainties in the position of the 24 tungsten cylinders along the radial and vertical direction, both in configuration  $C_1$  and  $C_2$ . Density inhomogeneities of the source masses have been modeled. An upper bound of the systematic uncertainty on  $G$  has been evaluated on the basis of the maximum density variation measured during the characterization of the tungsten cylinders. The contribution of the platforms holding the source masses has been included as well. The velocity of the atomic clouds and their position at the time of the first interferometer pulse have been calibrated performing time-of-flight measurements

Systematic effect	$\Delta G/G (\times 10^{-4})$
Radial position	1.2
Vertical position in $C_1$	2.7
Vertical position in $C_2$	2.1
Cylinders mass	0.9
Cylinders density inhomogeneity	0.21
Support platforms mass	0.8
Initial position of the atomic clouds	0.18
Initial velocity of the atomic clouds	2.3
Gravity gradient	1
Stability of the on-axis B-field	0.3
Stability of the launch direction	0.6
Total	4.6

TABLE I: Error budget of the systematic shifts affecting the  $G$  measurement.

and detecting the atoms when crossing a horizontal light sheet twice, once on the way up and once on the way down. The knowledge of the gravity gradient is also important to identify the best positions for the apogees of the two atomic clouds with respect to the source masses (see Fig. 2). Finally, special care has to be taken of all the systematic errors that could depend on the source masses distribution. For instance, the presence of an inhomogeneous magnetic field along the vertical axis depending on the position of the source masses can introduce a systematic phase shift affecting the  $G$  measurement. However, the low magnetic susceptibility of the tungsten alloy and the two  $\mu$ -metal shields surrounding the interferometer region ensure an excellent control of stray fields and reduce possible systematic errors below the measurement sensitivity of our apparatus. Using a tiltmeter, we have verified that the direction of the Raman lasers, which defines the sensitive axis of our interferometer, is stable within  $1 \mu\text{rad}$  and does not depend on the position of the source masses. At the same time, the stability of the launch direction has been evaluated and an upper bound on possible phase shifts induced by the Coriolis acceleration on the differential measurement estimated.

After an analysis of the error sources affecting our measurement, we obtain a value of  $G = 6.667 \cdot 10^{-11} \text{ m}^3 \text{ kg}^{-1} \text{ s}^{-2}$ , with a statistical uncertainty of  $\pm 0.011 \cdot 10^{-11} \text{ m}^3 \text{ kg}^{-1} \text{ s}^{-2}$  and a systematic uncertainty of  $\pm 0.003 \cdot 10^{-11} \text{ m}^3 \text{ kg}^{-1} \text{ s}^{-2}$ . Figure 4 shows this result and compares it to the most precise  $G$  values recently obtained in different experiments. Our measurement is consistent with the 2006 CODATA value within one standard deviation.

We have reported a new measurement of the Newtonian constant of gravity based on atom interferometry. This technique, completely different from the methods used to date, explores new systematics, globally improv-

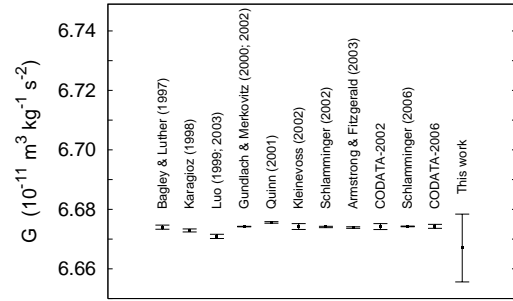


FIG. 4: Our result of the Newtonian gravitational constant compared to the most precise  $G$  measurements recently obtained and to CODATA recommended values.

ing the confidence in the knowledge of  $G$ . Presently, our statistical error averages down reaching a value comparable to the systematic uncertainty in about one day of integration time. As expected, the main contribution to the systematic error on the  $G$  measurement derives from the positioning accuracy of the source masses. This error will be reduced by about one order of magnitude once the position of the tungsten cylinders will be measured by a laser tracker. From the analysis of systematic effects and the characterization of the stability of our apparatus, we foresee interesting perspectives for pushing the measurement accuracy below the 100 ppm level.

This work was supported by INFN (MAGIA experiment), MIUR, ESA, and EU (under contract RII3-CT-2003-506350). G.M.T. acknowledges seminal discussions with M.A. Kasevich and J. Faller and useful suggestions by A. Peters. M. Fattori, T. Petelski, and J. Stuhler contributed to the setting up of the apparatus. We are grateful to A. Cecchetti and B. Dulach of INFN-LNF for the design of the source masses support and to A. Peuto, A. Malengo, and S. Pettorosso of INRIM for density tests on W masses.

\* Guglielmo.Tino@fi.infn.it

- [1] J. H. Gundlach and S. M. Merkowitz, Phys. Rev. Lett. **85**, 2869 (2000); T. J. Quinn et al., Phys. Rev. Lett. **87**, 111101 (2001); T. R. Armstrong and M. P. Fitzgerald, Phys. Rev. Lett. **91**, 201101 (2003); J. Luo and Z. K. Hu, Class. Quantum Grav. **17**, 2351 (2000); C. H. Bagley and G. G. Luther, Phys. Rev. Lett. **78**, 3047 (1997); O. V. Karagioz et al., Grav. Cosmol. **4**, 239 (1998).
- [2] S. Schlamminger et al., Phys. Rev. D **74**, 082001 (2006).
- [3] J. P. Schwarz et al., Science **282**, 2230 (1998).
- [4] W. T. Ni et al., Meas. Sci. Technol. **10**, 495 (1999).
- [5] U. Kleinevoss et al., Meas. Sci. Technol. **10**, 492 (1999).
- [6] A. Peters et al., Nature **400**, 849 (1999).
- [7] J. M. McGuirk et al., Phys. Rev. A **65**, 033608 (2002).
- [8] T. L. Gustavson et al., Phys. Rev. Lett. **78**, 2046 (1997).

- [9] B. Canuel et al., Phys. Rev. Lett. **97**, 010402 (2006).
- [10] S. Fray et al., Phys. Rev. Lett. **93**, 240404 (2004).
- [11] G. Ferrari et al., Phys. Rev. Lett. **97**, 060402 (2006).
- [12] P. Cladé et al., Phys. Rev. Lett. **96**, 033001 (2006).
- [13] H. Müller et al., Appl. Phys. B **84**, 633 (2006).
- [14] G. M. Tino et al., Nucl. Phys. B (Proc. Suppl.) **166**, 159 (2007).
- [15] A. Bertoldi et al., Eur. Phys. J. D **40**, 271 (2006).
- [16] J. B. Fixler et al., Science **315**, 74 (2007).
- [17] M. Kasevich and S. Chu, Phys. Rev. Lett. **67**, 181 (1991).
- [18] M. Kasevich and S. Chu, Appl. Phys. B **54**, 321 (1992).
- [19] G. Lamporesi et al., Rev. Sci. Instrum. **78**, 075109 (2007).
- [20] L. Cacciapuoti et al., Rev. Sci. Instrum. **76**, 053111 (2005).
- [21] G. T. Foster et al., Opt. Lett. **27**, 951 (2002).